Journal of Theoretical and Applied Mechanics, Sofia, Vol.51 (2021) pp. 242-273

In memory of JORDAN G. BRANKOV

TASEP ON NETWORKS WITH NONTRIVIAL GEOMETRY CONSISTING OF COUPLED SIMPLE LINEAR CHAINS

NADEZHDA BUNZAROVA, NINA PESHEVA*

Instititute of Mechanics, Bulgarian Academy of Sciences

[Received: 22 March 2021. Accepted: 29 March 2021]

ABSTRACT: We briefly overview some of our recent advances in the study of non-equilibrium phenomena with emphasis on steady state properties of the totally asymmetric simple-exclusion process (TASEP) defined on an open network containing a double-chain section in the bulk (i.e., a network, having a bifurcation and merging points). We consider different possible scenarios for the specific realizations of the network falling in two basic cases – the double-chain section consisting of chains with equal or different lengths. We refer to the latter case as a shortcut in the bulk. The phase compositions of these types of networks, depending on the rates of input and output of particles at the open ends, the conditions for occurrence of traffic jams and their properties, were determined by using both theoretical and numerical methods. We concisely present the simple theory of Effective Rates Approximation by the help of which, ignoring the correlations at the junctions of the chain segments, the possible phase structures of the network models are found.

KEY WORDS: TASEP; non-equilibrium phase transitions; non-equilibrium statistical physics; traffic flow models; kinetics of protein synthesis; Molecular motors traffic.

1 INTRODUCTION

Non-equilibrium statistical mechanics is considered one of the biggest unresolved challenges in theoretical physics (see, for example Refs. [1, 2]). This is one of the reasons for the very intensive study of simple non-equilibrium models in the last 35 years. True equilibrium processes are rare, they are a kind of idealization, since the surrounding world abounds with non-equilibrium processes. Moreover, some properties of nonequilibrium systems have no analogues in the equilibrium case. Non-equilibrium phenomena occur generally either when a system is relaxing towards an equilibrium state, or when it is kept out of equilibrium by applying external forces. Presently, the following features are considered as characteristic of the complex non-equilibrium behavior: phase transitions between stationary states of one-dimensional systems driven by boundary conditions; spatiotemporal pattern formation, including

*Corresponding author e-mail: nina@imbm.bas.bg

surface growth and density waves; generic long-range correlations due to conservation of current; anomalous diffusion.

However, our modern understanding of non-equilibrium systems is still far behind our knowledge and understanding of equilibrium systems, and the fundamental understanding and theoretical classification of non-equilibrium steady states is still incomplete. The importance of developing a fundamental and comprehensive theory of systems far from equilibrium was recognized quite a long time ago by Katz, Lebowitz and Spohn in [3, 4], where the special class of simple lattice-gas models driven far from equilibrium – the so called driven diffusive systems, was introduced. In these models, the particle dynamics is specified by stochastic hopping rules to nearest vacant sites with biased rates that simulate the action of an external field or a thermodynamic force.

When we are studying systems far from equilibrium, simplified models that can be solved exactly are of a particular importance. One such model is the Asymmetric Simple Exclusion Process (ASEP), which is a 1D lattice gas of hard-core particles on a chain that can move with a certain probability to a nearest neighbor vacant site. This model reduces to the totally ASEP (TASEP) when particles are allowed to move in one direction only. These processes (ASEP and TASEP) are among the simplest models of self-driven many-particle systems with particle conserving stochastic dynamics exhibiting phase transitions between three non-equilibrium stationary phases. ASEP and TASEP became paradigmatic models for understanding the broad variety of non-equilibrium phenomena, much like the Ising model in the study of equilibrium phase transitions.

TASEP was first suggested by MacDonald, Gibbs, and Pipkin [5] as a model of the kinetics of protein synthesis. Independently, TASEP was studied from mathematical viewpoint as an example of interacting Markov processes by Spitzer [6]. Later, the process found a number of applications: in biological transport [7,8], vehicular traffic flow [9, 10], forced motion of colloids in narrow channels [11–13], surface growth [14], transport of data packets on the internet, etc. In 1992 Nagel and Schreckenberg devised an improved model of vehicular single-lane traffic [15] which reduces to the TASEP with parallel update for special values of the parameters (when maximum vehicle velocity v_{max} =1).

The interest in TASEP grew immensely when its exact (in the limit of infinite chain) solvability was established. The first exact solution for TASEP with continuous-time dynamics on a simple chain was obtained at special values of the parameters by Derrida, Domany, and Mukamel [16], and shortly after that generalized to all values by Schtz and Domany [17].

In the general case of TASEP with continuous time, the exact stationary states have been obtained with a Matrix Product Ansatz (MPA) by Derrida, Evans, Hakim,

and Pasquier in 1993 [18]. The MPA formalism has been extended to the TASEP endowed with different types of discrete-time dynamics: sublattice-parallel (Hinrichsen, 1996) [19], sequentially ordered (Rajewsky, Schadschneider, and Schreckenberg, 1996) [20]. The most difficult case of parallel update was solved in 1999 by Evans, Rajewsky, and Speer [21], and, with a different Ansatz, by de Gier and Nienhuis [22]. As predicted by Krug [23], the change of the boundary rates induces non-equilibrium phase transitions between different stationary phases. For reviews on exactly solvable models of stochastic particle systems far from equilibrium see Refs. [24, 25].

In the last 20 years an intensive research on non-equilibrium systems is continuing, however, the emphasis in these studies is on more complex variants of TASEP, aiming at modeling more realistic systems. For example, different variants of TASEP and TASEP-like models are studied, having different kinds of inhomogeneities – like slow bonds [26, 27], site disorder [28, 29], dynamic defects [30, 31], or presence of branching and merging points, which introduced study of TASEP on networks [32–39]. Similarly, TASEP with additional interactions were suggested and studied – the generalized TASEP [40–48], and, e.g., [49, 50]. We mention here also, generalizations of TASEP, which were motivated by some applications to biological transport, e.g., the case when the entry rate is chosen to depend on the number of particles in the reservoir (the TASEP with finite resources) [51], the cases of multiple competing TASEPs with a shared reservoir of particles [52], and with limited reservoirs of particles and fuel carriers [53] were studied too, etc.

We have studied the stationary properties of nontrivial TASEP networks, containing bifurcation and merging points, modeled by the insertion of a double-chain section in the bulk of a linear backbone. The double-chain section may consist of chains with equal or different lengths. To the latter case we refer as a shortcut in the bulk. A natural interpretation of TASEP is especially clearly given in terms of a single-lane vehicular traffic. New applications of TASEP have been pointed out [54] which include also biophysical phenomena, which can take place on open networks with a nontrivial topology. It has been suggested that crowding of motor proteins, that can occur on such networks, may be responsible for some human diseases. Such networks simulate the motion of molecular motors along microtubules with varying number of protofilaments. Crowding phenomena can occur also when molecular motors move along twisted protofilaments. In such cases the molecules can jump with some probability between sites very distant along the backbone filament but close in real space (a shortcut of zero length).

In what follows we review some of our results on the stationary properties of nontrivial TASEP networks, containing bifurcation and merging points. First, we briefly recount some of the basic properties of the standard TASEP on simple chains.

Next, we consider the properties of TASEP on chains with a double-chain section in the middle, when the two middle (parallel) chains are of equal length [32, 33]. We review the main points of the Effective Rates Approximation method introduced in [32] to determine the phase structure of these types of networks. This method is also applied to the study of TASEP on chains with a double-chain section in the middle, where the double-chain section has been translated forward or backward, thus inducing a phase change in the chains of the double section [36,37]. We consider also the effect on the double-chain section in the network, when the length of the two end chains is changed. The last subsection is devoted to the appearance of traffic jams in a long chain with a shortcut in the bulk [38, 39].

2 Simple 1D TASEP – Some Known Results and Properties

Exactly solved models of driven diffusive systems can be obtained by switching off the interparticle interaction, leaving only the hard-core on-site exclusion and the external drive. The Totally Asymmetric Simple Exclusion Process is a 1D lattice gas of hard-core particles on a chain of L sites (the sites may be empty or singly occupied – $\tau_i = 0, 1$ for $i = 1, \ldots, L$) endowed with a stochastic dynamics. The continuous-time stochastic dynamics is modeled in computer simulations by the so called random-sequential update: the algorithm chooses with equal probability any one of the lattice sites (the left reservoir is included as an additional site), and, if the chosen site is occupied by a particle, moves it with probability p to the nearest-

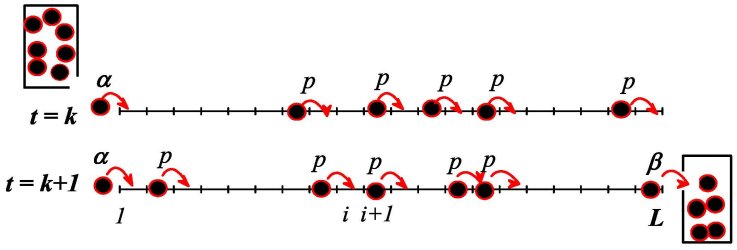

Fig. 1: Schematic representation of the update rules for one-dimensional TASEP at two time steps $t = k, k + 1$. Due to the hard core exclusion interaction between the particles at every site $i = 1, \ldots, L$ (for a finite system of L sites) there can be only one particle, i.e., $\tau_i = 0, 1$. Particles are injected at the left end with probability α and removed at the right end with probability β. In the bulk of the system particles may move one site to the right with probability p, provided the NN site on the right is empty.

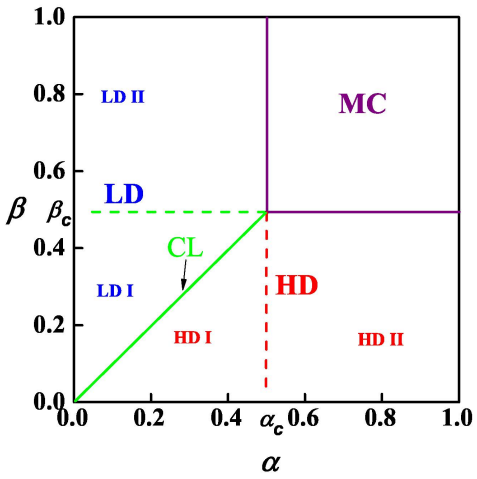

Fig. 2: Phase diagram of the one-dimensional TASEP as a function of the injection and ejection rates, α and β , respectively. It has three stationary phases: low density (LD) phase, consisting of sub-regions LDI and LDII (i.e., LD=LDI U LDII); high density (HD) phase (i.e., HD=HDI U HDII) and maximal current (MC) phases. The LD and the HD phases are separated by the coexistence line (CL). The sub-regions LDI (HDI) and LDII (HDII) differ by the bending of the density profile close to the exit (entry) point.

neighbour (NN) site on the right, provided the target site is empty. In the case of open systems, particles are injected at the left end with rate α and removed at the right end with rate β. When $\alpha, \beta \in (0, 1]$ the boundary conditions correspond to coupling of the system to reservoirs of particles with constant densities α and $\beta - 1$, respectively.

The model properties are determined by the choice of boundary conditions [23]. In the thermodynamic limit, the open system exhibits three distinct phases in the plane of particle input-output rates [16–18], shown in Fig. 2, with continuous or discontinuous in the bulk density (ρ_b) transitions between them. These phases are: a low density (LD) free-flow phase, a high-density (HD) congested traffic one, and a maximum current phase (MC), characterized by a synchronized flow in which jams and free-flow coexist at intermediate densities.

The stationary phases of the TASEP can be also identified with respect to the analytic form of the bulk current: for fixed p, the current J in the low- (high-) density phase depends only on $\alpha(\beta)$, and in the maximum-current phase it is independent of both α and β. On crossing the borderline between the maximum current and the low- (high-) density phase, the current itself and its first derivative with respect to $\alpha(\beta)$ change continuously and the second derivative with respect to $\alpha(\beta)$ undergoes a finite jump. The phase transition between the LD and HD phases is of first order (the bulk density and the first derivative of the current have finite jumps). These phases are separated by a coexistence line (CL), on which a shock phase (SP) with a delocalized Domain Wall (DW) takes place [55, 56]. The second-order phase transitions take place on the border line between the LD and the MC and also between the HD and the MC phases.

For a simple chain of $L \gg 1$ sites with injection (ejection) rates $\alpha(\beta)$ the following results hold:

In the low-density phase (LD), $\alpha < 1/2$, $\alpha < \beta$,

$$J = \alpha(1-\alpha)\,, \quad \rho_b = \alpha\,, \quad \rho_1 = \alpha\,, \quad \rho_L = \frac{\alpha(1-\alpha)}{\beta}\,. \tag{2.1}$$

In the high-density phase (HD), $\beta < 1/2$, $\beta < \alpha$,

$$J = \beta(1-\beta)\,, \quad \rho_b = 1-\beta\,, \quad \rho_1 = 1 - \frac{\beta(1-\beta)}{\alpha}\,, \quad \rho_L = 1-\beta\,. \tag{2.2}$$

In the maximum current phase (MC), $\alpha, \beta > 1/2$,

$$J = \frac{1}{4}\,, \quad \rho_b = \frac{1}{2}\,, \quad \rho_1 = 1 - \frac{1}{4\alpha}\,, \quad \rho_L = \frac{1}{4\beta}\,. \tag{2.3}$$

On the coexistence line (CL), $\alpha = \beta < 1/2$, the local density profile changes linearly from $\rho_1 = \alpha$ to $\rho_L = 1-\alpha$, i.e.,

$$\rho_{\mathrm{CL}}(i) = \rho_- + (\rho_+ - \rho_-)\frac{i}{L+1}\,, \tag{2.4}$$

where by ρ_- and ρ_+ the bulk densities in the low and high density phases are denoted. The nearest-neighbor correlations in this phase have a characteristic parabolic shape. According to the domain wall theory [55,56], the configurations of TASEP on a long simple chain (at $\alpha = \beta < 1/2$) can be approximated by two regions, of low and high density, separated by a domain wall of zero width.

The fundamental diagram of TASEP has a characteristic parabolic shape, determined by the dependence of the current J in the system on the bulk particle density ρ : $J = \rho(1-\rho)$ (see the empty circles – solid line curve in Fig. 6).

The TASEPs with different stochastic updates have the same phase structure and the relations between the current J and the bulk density ρ for TASEP under different updates were established in [57]. For a review on the exact results for the stationary states of a TASEP, under different kinds of stochastic dynamics, and its numerous applications, we refer the reader to [24,58].

3 TASEP on Networks with a Nontrivial Topology (Having Bifurcation and Merging Points)

Recently, much attention has been paid to TASEP on networks with a nontrivial topology. Such models allow one to study many diverse processes in the surrounding world, which are of a great interest. For example, most transport processes take place on networks with points of bifurcation, merging or crossing of several lanes. TASEP on such networks exhibits novel and unexpected properties (some of these

will be presented in the rest of this section). In vehicular traffic, junction points may cause traffic jams. Also, in biophysics, experiments have revealed that the number of protofilaments may vary, which indicates the existence of junctions and other lattice defects. Such defects might lead to motor proteins crowding phenomena that are responsible for many human diseases [54]. That is why the study of TASEP on networks is very important in so many aspects.

3.1 TASEP ON CHAINS WITH A DOUBLE-CHAINS SECTION IN THE MIDDLE, WHERE THE MIDDLE CHAINS ARE OF EQUAL LENGTH

The special case of a TASEP (with random sequential update) on a network with a section of two parallel chains of equal length, inserted in the middle of a long chain with open boundaries, was studied in our papers [32, 33] both analytically and by extensive Monte Carlo simulations. This network, presented schematically in Fig. 3, has two points of inhomogeneity. The last site of the head chain ($i = L_1$) is a branching point P_b from which particles can move along the upper or lower chain of the double chain section in the middle of the system with the same probability $q = 1/2$. Particles at the last sites of the two middle branches C_2 and C_3 may enter with equal probability the first site of the last network segment C_4, which is the merging point P_m of the network, i.e., $i = L_1 + L_2 + 1$.

TASEPs on networks with non-trivial topology are not exactly solvable. In order to treat analytically such systems we have proposed in [32] a method for theoretical analysis of the phase structure of the system, which we named the *Effective Rates Approximation* (ERA). Now ERA is widely used in investigation of complx networks

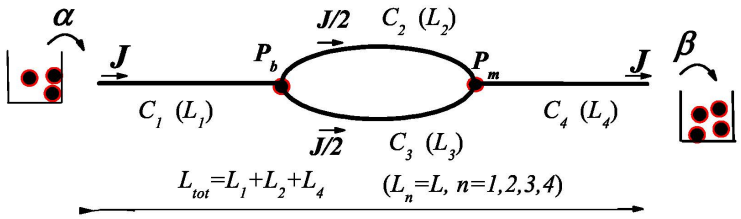

Fig. 3: Schematic representation of the open network with double-chain section in the middle. It has two inhomogeneity points P_b (branching point) and P_m (merging point). All simple chain segments C_n, $n = 1, \ldots, 4$, have equal length ($L_1 = L_2 = L_3 = L_4 = L$). The particles are injected at the left end with a rate α and removed at the right end with a rate β. The particles move from left to right as in the one-dimensional TASEP with random sequential dynamics. At the branching point P_b they take with equal probability ($q = 1/2$) the upper L_2 or the lower branch L_3.

(see, e.g., [54,59–62]). ERA is essentially a new method for analyzing networks with non-trivial topology and open boundaries. With its help, it was established that the presence of a middle section of two parallel chains leads to complex phase structures of the stationary state of the whole chain.

The following assumptions are at the core of the *Effective Rates Approximation*:

(1) TASEP on each of the long linear chain segments C_n, $n = 1, 2, 3, 4$, exhibits the stationary state properties of a single chain, and one can use, as a good approximation, the exact results obtained in the thermodynamic limit;

(2) The phase of each simple chain segment C_n is determined by its effective injection α_n^* and ejection β_n^* probabilities.

The possible phase structures of the complex network, shown in Fig. 3, are established at two successive levels of theoretical analysis.

At the first level of analysis, one takes into account only the exact results for a simple chain with open boundaries in the thermodynamic limit. Thus, in this case the pair correlations between nearest-neighbor sites vanish in the bulk. Using the continuity of the current through the network and also that the current $J(\rho)$, through a chain with a bulk density ρ, is given by $\rho(1-\rho)$ one has the following chain of relations:

$$J = \alpha(1 - \langle\tau_1\rangle) = \rho^{(1)}(1-\rho^{(1)}) = 2\rho^{(2,3)}(1-\rho^{(2,3)}) = \rho^{(4)}(1-\rho^{(4)}) = \beta\langle\tau_{3L}\rangle\,. \tag{3.1}$$

Here $\rho^{(n)}$ is the bulk density in the chain segment C_n, and $\langle\tau_i\rangle$ is the steady-state particle density at site i. We analyze in detail the possible phase structures, using 1) the relations (3.1); 2) our knowledge about single chain TASEP; and 3) keeping in mind that whenever a chain segment may be in both a low- and high-density phase under given values of the rates α and β, it may also be on the coexistence line between these two phases. Despite that, the analysis does not allow sufficient information to be derived on the phase structure of the system. That is why, at the next level of approximation we ignore the correlations between the chain segments, which make it possible to define the effective injection and/or removal rates α_n^* and β_n^* at the junctions of the simple chains.

At the second level, we assume that the following pairs of random variables are independent: $\langle\tau_{L_1}\rangle$ and $\langle\tau^{(2,3)}_{L_1+1}\rangle$, as well as $\langle\tau^{(2,3)}_{L_1+L_2}\rangle$ and $\langle\tau_{L_1+L_2+1}\rangle$.

Neglecting the corresponding correlations leads to an approximate expression for the total flow and for the chain under consideration, we obtain

$$\begin{aligned} J = \alpha\langle\tau_1\rangle &\approx \frac{1}{2}\langle\tau_{L_1}\rangle(1-\langle\tau^{(2)}_{L_1+1}\rangle) + \frac{1}{2}\langle\tau_{L_1}\rangle(1-\langle\tau^{(3)}_{L_1+1}\rangle \\ &\approx (\langle\tau^{(2)}_{L_1+L_2}\rangle + \langle\tau^{(3)}_{L_1+L_2}\rangle)(1-\langle\tau_{L_1+L_2+1}\rangle)\,. \end{aligned} \tag{3.2}$$

Thus, similarly to a simple chain, one can define the following effective rates α_n^* and β_n^* for the chain segments C_n

$$
\begin{aligned}
&(\alpha_1^* = \alpha)\,, && \beta_1^* = 1 - \langle \tau_{L_1+1}^{(2,3)} \rangle\,, \\
&\alpha_{2,3}^* = \frac{1}{2}\langle \tau_{L_1} \rangle\,, && \beta_{2,3}^* = 1 - \langle \tau_{L_1+L_2+1}^{(2,3)} \rangle\,, \\
&\alpha_4^* = 2\langle \tau_{L_1+L_2}^{(2,3)} \rangle\,, && (\beta_4^* = \beta)\,.
\end{aligned}
\tag{3.3}
$$

The possible phase structures of the whole network are obtained as solutions of the resulting set of equations for the effective rates that follow from the continuity of current. However, determining the possible phase structures is not so obvious, because not all possible combinations will appear, since the flow passing through the middle branches of the chain is equal to half the flow passing through the head and tail segments. More precisely, since the current in the system is $J = \rho(1-\rho)$ and the same value of the current $J < J^{\max} = 1/4$ can be supported by two different bulk densities

$$
\rho_{\pm}(J) = \frac{1}{2}[1 \pm (1 - 4J)^{1/2}]\,. \tag{3.4}
$$

Thus, for macroscopic chains the middle branches may never be found in the maximum-current phase.

We denote the expected phase structure of our model by the triplet $\{X_1,\, X_{2,3},\, X_4\}$, where $X_n \in$ (LD, HD, MC, CL) denotes the stationary phase of the chain segment C_n, $n = 1, 2, 3, 4$, where LD stands for the low density phase, and HD and MC to the high density and maximum-current phases, respectively, on the chain segment C_n.

Thus, the refined theoretical analysis of the allowed phase structures in our network with a nontrivial topology, based on the neglect of the pair correlations between the nearest-neighbor occupation numbers belonging to different chain segments, yields the following eight possibilities:

(3.5) A. When $\alpha < 1/2$ and $\alpha < \beta$ — (LD, LD, LD);

B. When $\beta < 1/2$ and $\alpha > \beta$ — (HD, HD, HD);

C. When $\alpha = \beta < 1/2$:

(LD, LD, HD), when $\alpha/2 < \langle \tau_{L_1+L_2}^{(2,3)} \rangle < \rho_+^{(2,3)}(\alpha)$;

(LD, HD, HD), when $\rho_-^{(2,3)}(\alpha) < \langle \tau_{L_1+1}^{(2,3)} \rangle < 1 - \alpha$;

(LD, CL, HD), when $\langle \tau_{L_1+1}^{(2,3)} \rangle = \rho_-^{(2,3)}(\alpha) = 1 - \langle \tau_{L_1+L_2}^{(2,3)} \rangle$;

D. When $\alpha > 1/2$, $\beta > 1/2$:

(MC, LD, MC), when $1/4 < \langle \tau^{(2,3)}_{L_1+L_2} \rangle < \rho^{(2,3)}_{+}$;

(MC, HD, MD), when $\rho^{(2,3)}_{-} < \langle \tau^{(2,3)}_{L_1+1} \rangle < 1/2$;

(MC, CL, MC), when $\langle \tau^{(2,3)}_{L_1+1} \rangle = \rho^{(2,3)}_{-} = 1 - \langle \tau^{(2,3)}_{L_1+L_2} \rangle$.

Below we present the results for the different phase structures found in the system (presented in Figs. 4 and 5) by numerical Monte Carlo simulations, which were performed for the considered network, for chain segments of equal number of sites $L = 200$. Note, that our computer simulations, show that whenever the chain segments of the middle section may exist in either the low- or high-density phases (as it is in cases C and D above), they are always found on the coexistence line.

CASE $\alpha < 1/2$ AND $\alpha < \beta$.
CASE $\beta < 1/2$ AND $\alpha > \beta$

As expected from our preliminary analysis, see **case A** above, the phase structure (LD, LD, LD) (shown in Fig. 4a), or respectively in **case B**, (HD, HD, HD) is realized (shown in Fig. 4b). The comparison of the theoretical predictions and the simulation results for the current and the bulk densities in the simple-chain segments shows that they agree fairly well, within expected finite-size and finite-sample corrections. The NN correlations ($F_{\text{corr}}(i, i+1) = \langle \tau_i \tau_{i+1} \rangle - \langle \tau_i \rangle \langle \tau_{i+1} \rangle$) obtained in the low (LD, LD, LD)- and high (HD, HD, HD)-density phases (not shown here) are characterized by short-range correlations appearing in the neighborhood of the bifurcation and merging sites of the network.

CASE $\alpha = \beta < 1/2$

Most interesting are the results of our computer simulations in this case. The expectation was to find the chain segments of the middle section on the coexistence line (see **case C** above), between the low-density phase with bulk density $\rho^{(2,3)}_{-}(0.25) \approx 0.1047$ and the high-density phase with bulk density $\rho^{(2,3)}_{-}(0.25) \approx 0.8953$. However, the simulations yielded values of the local density at the ends of these segments different from the predicted: at $i = L_1 + 1$ it is higher than the theoretical prediction and at the other end – $i = L_1 + L_2$ it is lower. The simulation results for the nearest-neighbor correlations (not shown here) reveal two important properties: first, strong correlations exist with parabolic spatial dependence in the chain segments of the middle section (indicative for phase coexistence with completely delocalized domain wall between the low- and high-density phases); second, rather strong correlations are also present in the head C_1 and tail C_4 chain segments away from the open boundaries.

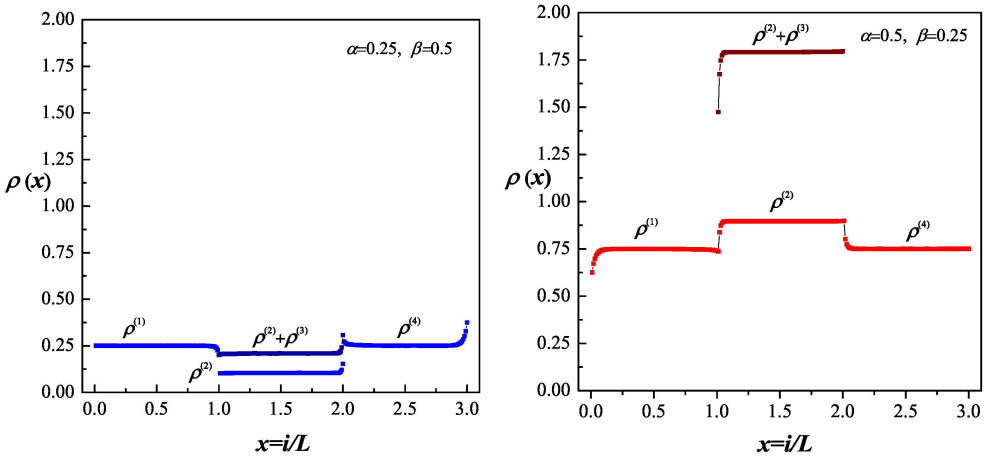

(a) (b)

Fig. 4: Local density profiles $\rho(x) = \langle \tau(i) \rangle$ (numerical simulations results) of particles in the system as a function of the normalized distance $x = i/L$, $x \in (0, 3]$, $i = 1, 2 \ldots, 3L$ when $L = 200$ sites: **(a)** at a phase point $\alpha = 0.25$, $\beta = 0.5$. The phase structure of the system is (LD, LD, LD) as expected from the theoretical analysis; **(b)** at a phase point $\alpha = 0.5$, $\beta = 0.25$. The phase structure of the system is (HD, HD, HD) as expected from the theoretical analysis. Note, in this case the density in the middle section $\rho^{(2)} + \rho^{(3)}$ exceeds unity.

The local density profiles on the coexistence line point to a novel phase structure. The equal slope of the head and tail segments C_1 and C_4 is smaller than in the middle chains C_2 and C_3. We have attempted to explain these features in the framework of the model of completely delocalized domain wall, however, taking into consideration the inhomogeneous structure of the considered network. Our theoretical predictions for shock phases in all four segments with different probabilities (for details see [32]) are shown by the dashed lines in Fig. 5a.

CASE $\alpha > 1/2$ AND $\beta > 1/2$

We find that the phase structure (MC, CL, MC) is realized in this case in the computer simulations out of the three possibilities, determined theoretically (see **Case D** above). The numerical simulation results for this phase structure are shown in Fig. 5b at phase point $\alpha = 0.75$, $\beta = 0.75$ (the whole network carries in this case the maximum current $J = 1/4$. We note, there is a deviation of the density profile in the chain segments of the middle section from a straight line between the densities $\rho_{-}^{(2,3)}$ and $\rho_{+}^{(2,3)}$ of the low- and high-density phases (as it should be in the shock phase),

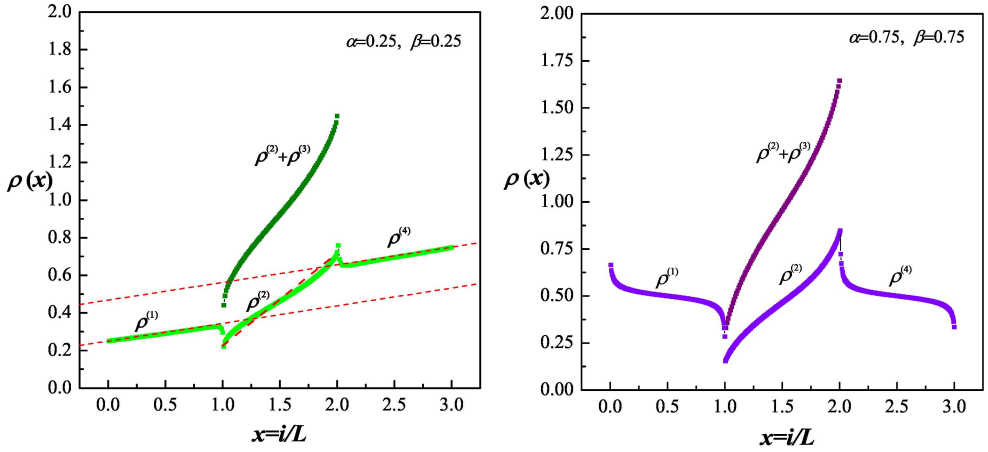

(a) (b)

Fig. 5: Local density profiles $\rho(x) = \langle \tau(i) \rangle$ in the network (from computer simulations) are shown as a function of the scaled distance $x = i/L$, $i = 1.2, \ldots, 3L$, when $L = 200$ sites: **(a)** at a phase point $\alpha = 0.25$, $\beta = 0.25$, where the system has the phase structure (LD, CL, HD). The (red) dashed lines show our analytical results from the application of the DW theory; **(b)** at a phase point $\alpha = 0.75$, $\beta = 0.75$, where the system has the phase structure (MC, CL, MC) of maximal current flowing in the system.

i.e., it has visible curvatures near the junction points. However, the obtained nearest -neighbor correlation function at $\alpha = \beta = 0.75$ (not shown here) has the characteristic parabolic shape in the parallel segments C_2 and $C_{3,}$ indicating that they are in the shock phase (on the coexistence line).

We end this subsection by showing the fundamental diagram of the network. It is calculated as follows: the left-hand side is obtained by varying $\alpha \in (0, 1]$ at fixed $\beta = 0.75$, and the right-hand side by varying $\beta \in (0, 1]$ at fixed $\alpha = 0.75$. The total bulk density in the network is defined as

$$\rho = \frac{1}{3} \sum_{n=1}^{4} \rho^{(n)} \,. \tag{3.6}$$

Figure 6 illustrates the two most remarkable effects of the presence of the double chain in the middle of a simple chain: at maximum flux values, a relatively wide plateau appears (when $0.3 \leq \rho \leq 1.1$) and bulk densities above unity exist. The latter feature is explained by its definition by Eq. 3.6, i.e., since in contrast to the simple-chain case, in our network the bulk density is inhomogeneous (see Fig. 6, where the total density in the two branches of the double-chain section exceeds unity).

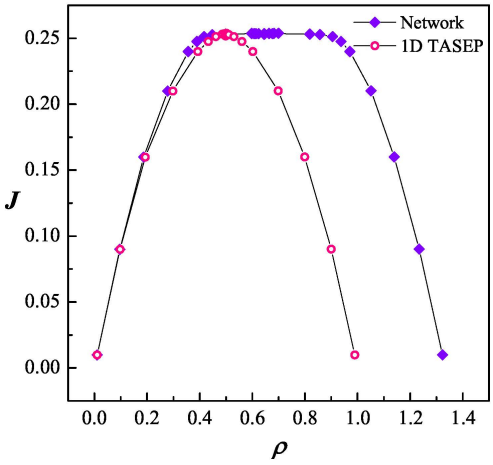

Fig. 6: The fundamental diagram for the considered network – the current as function of the bulk density in the system $J(\rho)$, obtained from the numerical simulations: the solid squares – solid line curve is the result for the system with a double-chain section in the middle; the empty circles – solid line curve is for a simple chain TASEP.

3.2 Effect of shifting the double-chain section from the central position forward or backward along the TASEP network

Here we continue with recounting new properties of TASEP, defined on an open network consisting of simple head and tail chains with a double-chain section in-between (as in Section 3.1), which ensue, however, when shifting the position of the double-chain section from the middle position – see Fig. 7, where schematic image of the system is presented. This variant of the network was studied in our works [33,34].

The possible phase structure of the present network is determined by the mean-field method, introduced in [32] and presented here in Section 3.1. We have shown there that the phase state of the chains in the double-chain section depends on the effective injection rate a_n^* of particles at the first site of each of the chain segments C_n and on the effective removal rate β_n^* of particles from the last site of each of these chains. In our studies of the present network we focused on the investigation of three of the most interesting cases (MC, LD, MC), (MC, CL, MC), and (MC, HD, MC) phase structures, appearing when the boundary rates satisfy the inequalities $\alpha > 1/2$ and $\beta > 1/2$ (for these values the simple chain TASEP is in the MC phase).

Results of Monte Carlo simulations of the system reveal a rather interesting property whenever the network with $L_{\text{tot}} = L_1 + L_2 + L_4$ has the {MC, CL, MC}phase structure. The effective rates a_2^*, β_2^* at the network junction points can be modified simply by changing the position of the double-chain section along the network, while keeping fixed both the total length L_{tot} of the network and the length $L_2 = L_3 = L_d$ of the double-chain section. This is clearly observable in Fig. 8. In the symmetric case of equal injection and ejection rates $\alpha = \beta > 1/2$ and equal lengths of the head and tail sections, the density profiles in the two parallel chains are almost linear,

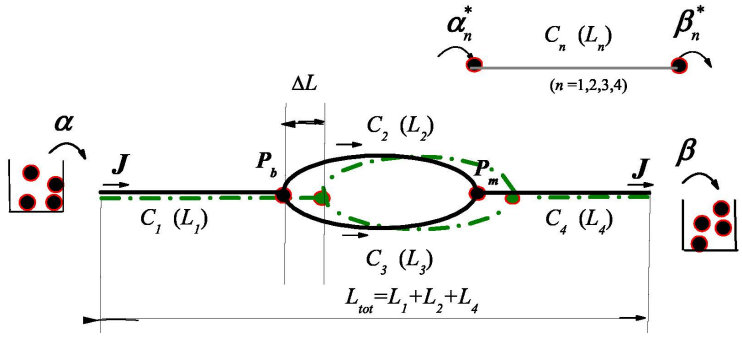

Fig. 7: Schematic presentation of the considered system: TASEP, defined on an open network (solid black line) with two inhomogeneities – branching P_b and merging P_m points. It consists of head C_1 and tail C_4 simple-chain TASEP segments with a double-chain section (comprising the branches C_2 and C_3 having equal lengths $L_2 = L_3 = L_d$) inserted betweenC_1 and C_4. (Note, in the open network system considered in Section 3.1 all the simple-chain segments C_i have equal lengths $L_1 = L_2 = L_3 = L_4 = L$). The olive green dash-dotted line shows a version of the network, where the double-chain section has been translated forward by ΔL, so that the head and tail simple-chain segments have lengths $L'_1 = L_1 + \Delta L$ and $L'_4 = L_4 - \Delta L$, while the whole network has the same total length $L_{\text{tot}} = L_1 + L_2 + L_4$.

characteristic of the coexistence line. As one can see in Fig. 8a, a simple translation forward of the double-chain section leads to a density profile on C_2 and C_3 characteristic of the LD phase (shown by empty right (cyan) triangles), while translation backward induces a density profile characteristic of the HD phase (shown by solid (red) rhombs). We refer to this transition as **position-induced phase change.** It affects the total number of particles in that part of the network. As a reference, also the results for the density profiles of the system with segments of equal length $L_1 = L_{2,3} = L_4 = 100$ are shown by empty (blue) up-triangles. The characteristic change of the density profiles is accompanied also by the corresponding characteristic change in the nearest-neighbor correlation function F_{corr} (not shown here). It is quite similar to that shown in Fig. 10a for a slightly different system, presented in the second part of this subsection.

Numerical studies of larger systems (e.g., with a total length of $L_{\text{tot}} = 300$ sites) reveals even higher sensitivity (e.g., compared to smaller systems of size $L_{\text{tot}} = 150$ sites) of the density distribution $\rho(x)$ along the chains C_2 and C_3 of the double-chain section with respect to quite small changes of its position in the network. Then the smooth phase transition in $C_{2,3}$ becomes sharper. The results shown in Fig. 8b are obtained after $N_{\text{tau}} = 3\,000\,000$ Monte Carlo steps are omitted in order to ensure

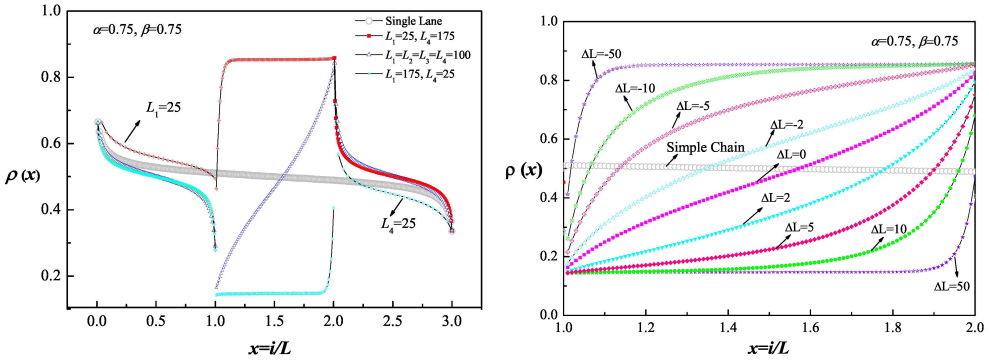

(a) (b)

Fig. 8: **(a)** Density distributions $\rho(x)$ (obtained from MC simulations) as a function of the scaled distance $x = i/L$ along the different chain segments of the open network, when $\alpha = 0.75$ and $\beta = 0.75$. The system total length is $L_{\text{tot}} = 300$. The empty (blue) up-triangles show the density distribution, characteristic for the system when all segments of the network have equal lengths $L_1 = L_2 = L_3 = L_4 = 100$ and the system has the (MC, CL, MC) phase structure. If the double-chain part is moved along the network forward and backward by $\Delta L = 25$ (while the lengths of both branches C_2 and C_3 are kept fixed at $L_2 = L_3 = 100$) this produces a noticeable change of the density profiles of C_2 and C_3: a translation forward (by $\Delta L = 25$) leads to a density distribution shape on C_2 and C_3 (shown by empty right (cyan) triangles) characteristic of the LD phase; a translation backward leads to a density distribution shape on C_2 and C_3 (shown by solid (red) rhombuses) characteristic of the HD phase. For completeness, the density distribution (in a MC phase with $\alpha = 0.75$ and $\beta = 0.75$) of a simple chain TASEP of length of $L_{\text{tot}} = 300$ sites is also shown by large open grey circles ($i = 1, 2 \ldots, L_n$ ($n = 1, 2, 3, 4$)); **(b)** Density distributions $\rho(x)$ (obtained from MC simulations) as a function of the scaled distance $x = i/L$ only on the middle branches for different values of the shift ΔL (i.e., for $\Delta L = 0, \pm 2, \pm 5, \pm 10, \pm 50$), illustrating how sensitive is the phase state of the middle branches even for small values of the shift ΔL.

that a stationary state of the system is reached and then ensemble averaging with $N_{\text{ens}} = 200$ of the results is performed.

An explanation of the described phenomenon of phase change, taking place on the chains $C_{2,3}$, is offered in terms of a finite-size dependence of the effective injection and ejection rates α_d^* and β_d^* at the ends of the double-chain section. Applying the approach (introduced in [32]), we have determined the effective rates α_d^* and β_d^* at the two ends of the double-chain section as a function of the actual average densities at

these sites. This help us to identify the possible phase structures of the system. However, there is a degree of freedom, due to the fact that the average density of particles in the chains $C_{2,3}$ is not fixed. One can deduce the missing injection and ejection rates from the fits of the simulated density profiles with the exponential distribution functions, predicted by the domain wall theory. For more details on this derivation see Refs. [37, 38].

In order to test the validity of the DW theory results, we made computer simulations of TASEP on a single chain using the injection and ejection rates α_d^* and β_d^* determined from the fitting of the density profiles on $C_{2,3}$ (obtained from the MC simulations). We explain the observable deviations of the density profiles from these of the infinite chain by the combined effect of the finite-size effects and the correlations appearing in the neighborhood of the points of inhomogeneity (P_b, P_m) of the network (see Fig. 3 in [38]). When the length of the chains is increased, this effect gets even stronger (see Fig. 4 in [38]).

Note, for the considered here network, the phase change in the middle chains $C_{2,3}$ is caused by the combined effect of the changes of both effective rates α_d^* and β_d^* at the two junction points of the network.

We have found also that the increase of the number of parallel chains in the inserted section (when the parallel chains are in the LD phase) the total bulk density of particles in them decreases to the value 1/4. This is so, since in the case of n parallel equivalent chains the current through each of them is $J^{\max}/n = 1/4n$. Using the relation between the current and the bulk density (valid for the low density phase)

$$\rho_-(J^{\max}/n) = \frac{1}{2}(1 - \sqrt{1 - n^{-1}})\,, \tag{3.7}$$

one obtains

$$n\rho_-(J^{\max}/n) = 1/4\,. \tag{3.8}$$

While when the parallel chains are in the HD phase the total bulk density in the n parallel chains, increases linearly with n, i.e.,

$$\rho_+(J^{\max}/n) = n - \frac{1}{4} + O(n^{-1}) \quad \text{as} \quad n \to \infty\,. \tag{3.9}$$

For the sake of completeness we show here also results from numerical simulations on a network of similar topology, however, with $L_1 = L_2 = L_3 = 50$ kept fixed and varying the length $L_4(L_1)$ of the last (first) segment $C_4(C_1)$ of the network. In this case, however, the total length L_{tot} of the network is not preserved.

The phase change on the chains $C_{2,3}$ for this realization of the network is also due to the finite-size dependence of the effective injection and ejection rates α_d^* and

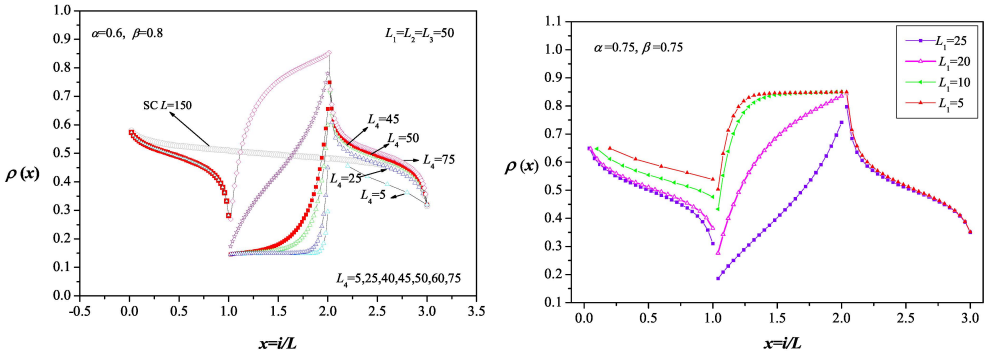

(a) (b)

Fig. 9: **(a)** The effect of changing the length L_4 on the density profiles of the middle parallel chains is illustrated: density distributions $\rho(x)$ (obtained from MC simulations) is shown as a function of the scaled distance $x = i/L$ along the different chain segments of the open network, when $\alpha = 0.6$ and $\beta = 0.8$. At this phase point the reference system, where all segments are of equal length $L_1 = L_2 = L_3 = L_4 = 50$ has the (MC, CL, MC) phase structure; **(b)** The effect of changing the length L_1 on the density profiles of the middle parallel chains is illustrated: density distributions $\rho(x)$ (obtained from MC simulations) is shown as a function of the scaled distance $x = i/L$ along the different chain segments of the open network, at the phase point $\alpha = 0.75$, $\beta = 0.75$. At this point the reference system, where all segments are of equal lengths $L_1 = L_2 = L_3 = L_4 = 25$ has the (MC, CL, MC) phase structure.

β_d^*. More precisely, when the length L_4 decreases from $L_4 = 50$ to $L_4 = 5$ (when the reference system, where all the segments have equal lengths $L_1 = L_2 = L_3 = L_4 = 50$, has the (MC, CL, MC) phase structure) one observes similar change of the phase of the double-chain section in the middle: starting from a density profile, characteristic of the CL phase, it changes to a density profile, characteristic of the LD phase. If, however, the length of L_4 is increased from 50 to 75 the opposite transition takes place, i.e., the density profiles of chain segments C_2 and C_3 take the shape of a profile, characteristic of HD phase. This effect can be observed in Fig. 9a, where numerical results from MC simulations for the density profile $\rho(x)$. One can achieve the same effect by changing also the length L_1 of the first chain segment while keeping the length of the two parallel chains and the last one $L_2 = L_3 = L_4 = 50$ fixed. If the length L_1 is decreased, however, this drives the two middle chains into a high density phase, while increasing the length L_1 drives them into a low-density phase (Fig. 9b).

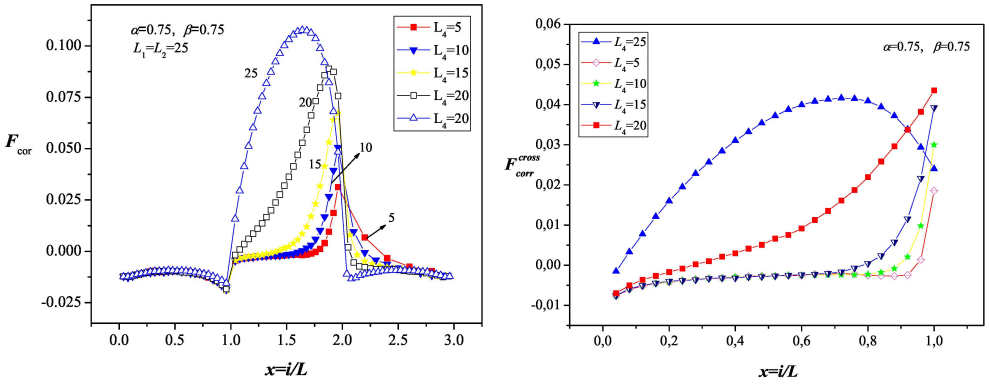

(a) (b)

Fig. 10: **(a)** The NN correlation function F_{corr} (MC simulation results) along the network when the length L_4 of the last (tail) simple chain is varied at phase point $\alpha = 0.75$ and $\beta = 0.75$ for a small system with $L_{\text{tot}} = 100$ sites. The results show the increased sensitivity of the NN correlation F_{corr} to even a very small change of the length of the last segment L_4 of the network. The solid up (blue) triangles are the reference results for $L_1 = L_2 = L_3 = L_4 = 25$ (i.e., when the system is in the (MC, CL, MC) phase structure); the empty (pink) rhombs show the result when $L_4 = 5$; **(b)** The cross-correlation function $F_{\text{corr}}^{\text{cross}}$ (MC simulation results) between the chain segments C_2 and C_3 (as function of the scaled distance $x = i/L, i = L_1 + 1, \ldots L_2$), when the length L_4 of the last (tail) simple chain is varied at phase point $\alpha = 0.75$ and $\beta = 0.75$ for a small system with $L_{\text{tot}} = 100$ sites. The cross-correlation function $F_{\text{corr}}^{\text{cross}}$ also is very sensitive to even a very small change of the length of the last segment L_4 of the network. The solid up (blue) triangles are the reference results for $L_1 = L_2 = L_3 = L_4 = 25$ (i.e., when the system is in the (MC, CL, MC) phase structure); the empty (pink) rhombs show the result when $L_4 = 5$.

The NN correlation function F_{corr} of the whole network are shown for different lengths of C_4 in Fig. 10a and the cross-correlation function $F_{\text{corr}}^{\text{cross}}$ (MC simulation results) between the chain segments C_2 and C_3 is shown in Fig. 10(b). One can see that both correlation functions display high sensitivity with respect to changing the last chain segment's length L_4.

In conclusion we note, that the phase change in the middle chains $C_{2,3}$ in this particular case (in difference to network considered in the beginning of this subsection) is triggered by the change of only one of the effective rates α_d^* or β_d^* at the two junction points of the network.

3.3 Totally asymmetric simple exclusion process on chains with a shortcut in the bulk

Motivated by the work of Y.-M. Yuan et al. [63] on TASEP model with zero-length shortcut and our results on the networks, presented in Sections 3.1 and 3.2, we decided to study the model by the ERA method. In particular we were interested in the case when in the system flows maximal current. Indeed, the TASEP with shortcut model (see the schematic image in Fig. 11b) can be viewed as a modified variant of the network, considered in Sections 3.1 and 3.2, however, when the two middle branches are not of equal length.

In our paper [38] we studied first the limiting case of zero-length shortcut and then the more general case of shortcut of arbitrary length [39] of driven lattice gases on networks with a shortcut. Novel features were obtained using the method of the effective rates.

In Biophysics, such models can describe the possibility of molecular motors, moving over long twisted filaments, to jump between sites close in space but far apart along the backbone (as depicted in Fig. 11a). In application to vehicular traffic, the results may suggest optimal solutions for planning of road shortcuts.

A. First, we have reconsidered the model with a zero-length shortcut, which was suggested by Y.-M. Yuan et al. [63] for the description of directed motion of molecular motors along twisted filaments. We found some unexpected results, which revise the previous findings in the case of maximum current through the network.

In principle, the effect of a shortcut can easily be understood: the shortcut takes a part of the current away from the second segment. Such a current can be supported by a chain either in a LD phase with $\rho_- = 1/2 - \sqrt{J^{\rm sc}}$, or in a HD phase with $\rho_+ =$

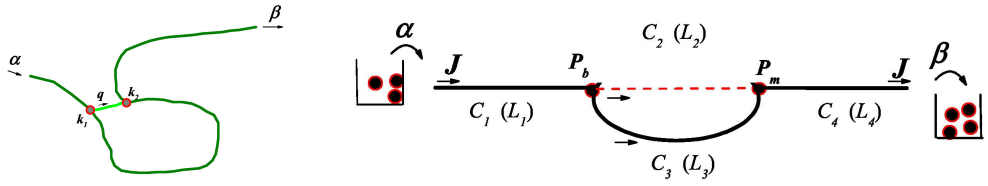

(a) (b)

Fig. 11: **(a)** The filaments in cells, on which the molecular motors move, may have irregular shapes (as shown in the figure) and a molecular motor may have a chance to jump with probability q directly to site k_2 from site k_1; **(b)** The respective schematic representation of the network geometry: TASEP with a shortcut. The three segments of the network are denoted by C_n, $n = 1, 3, 4$. The shortcut (C_2) is shown by a dashed green line $(L_2 < L_3)$. The shortcut may have even zero length.

$1/2 + \sqrt{J^{\rm sc}}$. The change in the current through the shunted part (segment C_3) of the original chain leads to a change of the particle density in the latter. Our theoretical analysis, based on ERA, shows that the shunted segment can exist in both low- and high-density phases, as well as in the coexistence (shock) phase. The numerical simulations show that the last option takes place in finite-size networks with head and tail chains of equal length, provided the injection and ejection rates at their external ends are equal and greater than one-half.

The model of TASEP on an open network, consists of 3 segments (C_1, C_3, and C_4) of L sites (see Fig. 11b). Zero-length shortcut allows a particle at the last site of the first segment C_1 to jump with a given probability $q = P_j$ directly to the empty first site of the last segment C_4.

In our numerical simulations we have taken $L_1 = L_3 = L_4 = 400$, and $\alpha = \beta = 0.75$, so that the current through the system takes its maximum value $J^{\max} = 1/4$. The stationary state of each segment is determined by the effective input, α_n^*, and output, β_n^*, rates for each segment n. The continuity of the current leads to a set of equations between these quantities (as described in Section 3.1). The solutions for α_n^*, and β_n^* determine the non-equilibrium stationary phase of each segment $n = 1, 3, 4$ and are determined by the following relations:

$$J^{(n)} = \beta_n^* \rho_L^{(n)} = \alpha_n^* (1 - \rho_1^{(n)}) \,, \quad \alpha_1^* = \alpha \,, \quad \beta_4^* = \beta \,, \tag{3.10}$$

where $J^{(n)}$ is the current through the segment n, $\rho_1^{(n)}$ and $\rho_L^{(n)}$ are the average local densities at the first and last (L^{-th}) site of that segment.

We have found that the shunted (C_3) segment is in the shock phase only when the rates $\alpha_3^* = \beta_3^*$, satisfy the cubic equation

$$4q(\alpha_3^*)^3 - 4(\alpha_3^*)^2 + (4+q)\alpha_3^* - 1 = 0 \,. \tag{3.11}$$

This equation shows, that the main quantitative parameters of that shock phase are governed by a positive root of a cubic equation, the coefficients of which linearly depend on the probability of choosing the shortcut.

Another problem of interest about the applicability of the domain wall theory (DW) to the central segments of the chain of our network, is not trivial. Segments are not connected to reservoirs of low and high density. The left ends are connected to the right and of the first segment, where the local density is $\rho_L^{(1)} = 1/4\beta_1^* < 1/2$, and their right ends are connected to the left and of the last segment, where the local density is $\rho_1^{(4)} = 1 - 1/4\alpha_4^* > 1/2$. These conditions differ from the connections to reservoirs in that there are significant correlations at the junctions between the segments, while such are absent in the case of reservoirs.

The predictions of the DW theory for the endpoints of the shunted segment are

$$\rho_{1,L}^{(3)} = \frac{1}{2} \mp \sqrt{J^{\rm sc}} \,. \tag{3.12}$$

An open chain with stationary current $J < 1/4$ can be found in low- high-density phases ($\rho_{\mp}(J)$). According to the domain wall theory [55, 56], on the coexistence line these phases are separated by a completely delocalized domain wall. As a result, the averaged density profile is linearly increasing from $\rho_{-}(J)$ at the left end of the chain to $\rho_{+}(J)$ at its right end.

Another important prediction of the domain wall theory is the parabolic shape of the nearest-neighbor correlations with the maximum value given by the following relation:

$$\max_x F_{\rm cor}(x) = \frac{[\rho_{+}^{(3)} - \rho_{-}^{(3)}]^2}{4} = \frac{1}{4} - J^{(3)} = J^{\rm sc} \,, \tag{3.13}$$

where $\rho_{\mp}^{(3)} = \rho_{\mp}(J^{(3)})$ with $\rho_{\mp}(J) = \dfrac{(1 \pm \sqrt{1-4J})}{2}$.

This finding has been verified by our computer simulations for all the values of the parameter q (taking into account that the current through the shortcut, $J^{\rm sc}$, depends on the probability q). The validity of this prediction of the domain wall theory is illustrated in Fig. 12.

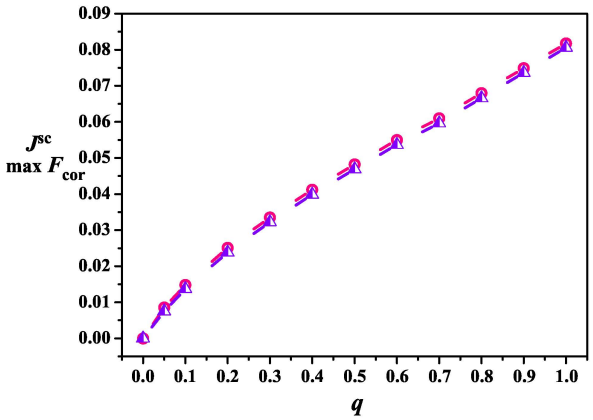

Fig. 12: The maximum of the nearest-neighbor correlations $\max_x F_{\rm cor}(x)$ along the shunted segment as function of q. The maximum of the nearest-neighbor correlations $\max_x F_{\rm cor}(x)$ (violet triangles) occurs near the midpoint of the shunted segment (C_3) and its value closely follows the prediction of the delocalized DW theory (pink circles).

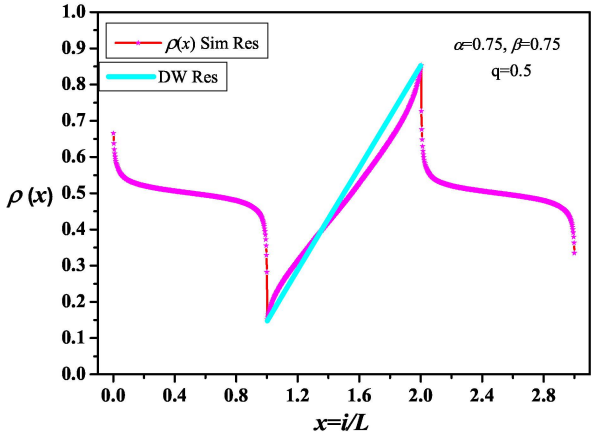

Fig. 13: The simulated local density profiles, $\rho(x)$, $x = i/L$, along the network ($L_1 = L_3 = L_4 = 400$) at $\alpha = 0.75$, $\beta = 0.75$ and $q = 0.5$ (in the case of zero length shortcut). In the shunted segment the almost linear profile (violet symbols) is compared to the delocalized DW prediction (cyan solid line).

Moreover, we have conjectured that these relations do not depend on the nature (structure) of the shortcut.

The simulated local density profiles along the network ($L_1 = L_3 = L_4 = 400$) in the case of zero length shortcut at $\alpha = 0.75$, $\beta = 0.75$ (on the diagonal in the domain of the maximum current phase of a single chain) and $q = 0.5$ are shown in Fig. 13. The almost linear density profile (violet symbols) on the shunted segment is compared to the delocalized DW prediction, shown by cyan solid line. The observed deviations are attributed to the correlations near the junction point, and, possibly, to finite-size effects. The abscissa x is as usual the normalized per L distance.

B. We also studied the dynamics of molecules on a twisted filament in the bulk in the case of a shortcut (bypass) with arbitrary length $L^{\rm sc}$. The second (C_2) chain representing the shortcut has length $L^{\rm sc}$, which varies from 2 to 100 sites. We considered the representative case when $q = 1/2$.

Our purpose was to analyze the conditions under which the shunted segment is in the coexistence phase and to check if the main features of the coexistence phase in that segment agree with the predictions of the DW theory. We also aimed to check if the main features of the coexistence phase in the shunted segment depend only on the current through the shortcut and do not depend on the length of the latter.

Our simulation results for the system at $\alpha = \beta = 0.75$ (i.e., when a maximum current flows in the system) are shown in Fig. 14 together with our DW predictions (cyan line).

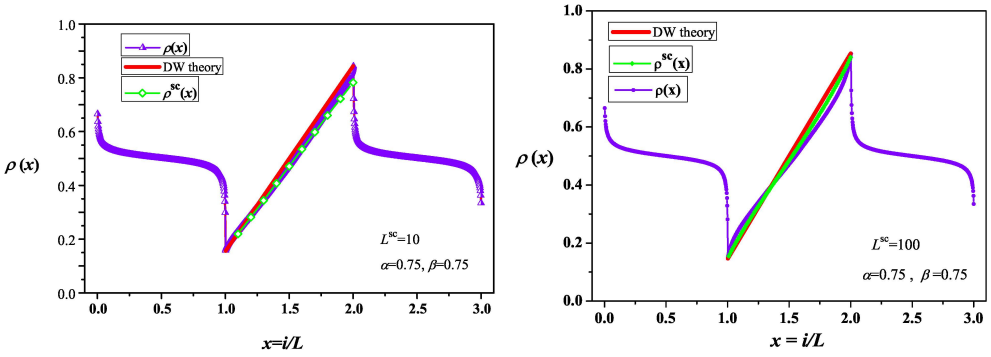

(a) (b)

Fig. 14: **(a)** Local density profiles, $\rho(x)$, $x = i/L$, (simulation results) in the network with $L_1 = L_3 = L_4 = 400$ sites for a shortcut of length $L^{\rm sc} = 10$ sites at $\alpha = \beta = 0.75$. One can see that the data of the computer simulations follows very closely the predictions of the DW theory (the cyan line); **(b)** The results for the local density profile in the case of a rather long bypass containing 100 sites ($L^{\rm sc} = L_2 = 100$ and $L_1 = L_3 = L_4 = 400$ sites). In this case, both the shunted segment C_3 and the bypass (C_2) are in the coexistence phase.

Under the random sequential update, the inter-chain correlations measure the difference between the actual current of particles and its mean-field approximation. The negative values of the inter-chain correlations $G_{1,3}$ and $G_{1,\rm sc}$, (see Fig. 15b, where results from MC simulations are shown), imply that the actual currents through the shunted segment and the shortcut exceed the corresponding mean field approximations at the bifurcation point, i.e., we have for the currents through the shunted segment through the shortcut:

$$J^{(3)} = q\left[\rho_L^{(1)}(1-\rho_L^{(3)}) - G_{1,3}\right], \tag{3.14}$$

$$J^{\rm sc} = (1-q)[\rho_L^{(1)}(1-\rho_1^{(\rm sc)}) - G_{1,\rm sc}\,. \tag{3.15}$$

Our results for the currents through the shunted segment and the shortcut are presented as functions of the length $L^{\rm sc}$ of the shortcut in Fig. 15a.

Having in mind our results for the network case studied in Section 3.2, here we also check what happens when the shortcut is shifted along the network. We find that due to the finite-size effects, for all values of the external rates in the domain of the MC phase, there exist a position of the shortcut for which the shunted segment is in a shock phase with a completely delocalized domain wall. The shift of the shortcut from this position toward the head or tail segment leads to a phase change

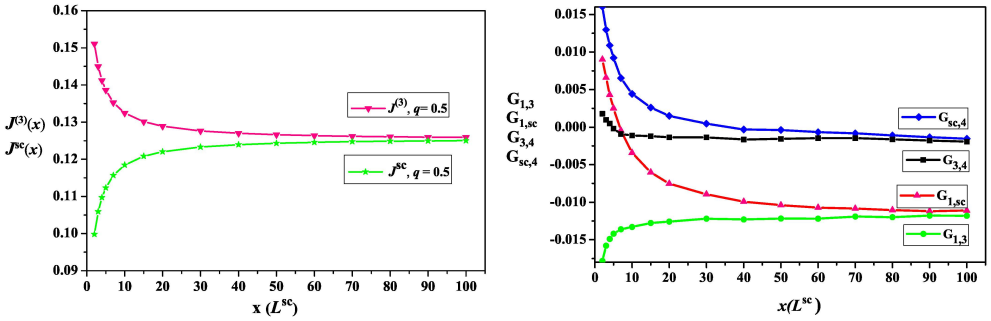

(a) (b)

Fig. 15: **(a)** The currents through the shunted segment (C_3) and the shortcut (C_2) as functions of the length of the shortcut $L^{\rm sc}$ after the correction of the corresponding mean-field value with the inter-chain correlation is made (see Eqs. (3.14) and (3.15)); **(b)** Estimated inter-chain correlations at the bifurcation and merging points. They are drastically different at small lengths of the shortcut, but as the latter grows, both correlations $G_{1,3}$ and $G_{1,\rm sc}$ approach the same value of about -0.01.

in the shunted section to a high-density phase or low-density phase, respectively (see Fig. 16, where simulation results for a system of $L_1 = L_3 = L_4 = 400$ sites at $\alpha = \beta = 0.75$ are presented and the shortcut is shifted forward by $\Delta L = 200$ sites and backwards by $\Delta L = -200$ sites).

We can summarize our main findings as follows:

(1) For any non-zero length of the shortcut and any values of the external rates in the domain of the maximum current phase, there exists a position of the shortcut where the shunted segment is in the coexistence phase with completely delocalized domain wall;

(2) The model displays some unexpected features: (a) the current through the shortcut is smaller than the current trough the longer shunted segment, and (b) the completely delocalized domain wall in the coexistence phase of the long shunted segment induces similar behavior even in shortcut containing a small number of sites;

(3) Under a shift of the shortcut to the head or tail of the network, the particle density profile in the shunted section drastically changes its shape from the one typical of a high-density phase to one typical of a low-density phase.

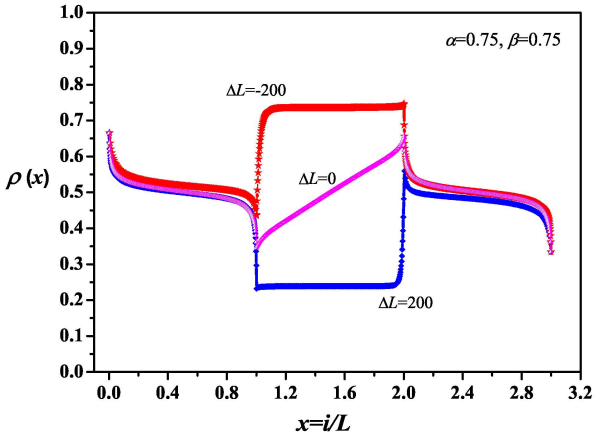

Fig. 16: Local density profiles, $\rho(x)$, $x = i/L$, (simulation results) at $\alpha = \beta = 0.75$ in a network with segments of length $L_1 = L_3 = L_4 = 400$. Upon shifting the shunted section forward ($\Delta L = 200$) or backward ($\Delta L = -200$) from the central position, the finite-size effects lead to $\alpha_3^* > \beta_3^*$ or $\alpha_3^** < \beta_3^*$ and the local density profile changes its shape from the one typical for the high-density phase to the one typical for the low-density phase, respectively.

4 Conclusion

This paper presents an overview of our main results obtained in past two decades in the investigation of the stationary non-equilibrium states of TASEP on finite open chains with nontrivial topology. With the aim to study TASEP models on the networks with complex geometry we have proposed and developed a well-functioning theory of the effective rate approximation (ERA). A key point of the method is the introduction of effective probabilities of input and output of particles on the simple chains, of which the entire network is composed. It turned out as a very useful tool in the study of a wide variety of characteristics of such networks. Currently, it is widely used by researchers in the study of such complex systems.

First, we introduced ERA in our study [32], where it was found that the presence of a middle section of two parallel chains of equal length, inserted in the middle of a simple chain TASEP, leads to complex phase structures of the stationary state of the whole network. By the help of ERA all possible phase structures were determined. In all possible phase structures of the system, the local profiles of the density of the number of particles, correlations between nearest neighbors along the constituent chains, and cross-correlations between equivalent sites belonging to two branches of the middle section were studied by means of computer simulations. When $\alpha =$

$\beta < 0.5$ (i.e., a CL phase appears in the 1D TASEP), clear signs of the presence of a delocalized domain wall, was found, which has different probabilities of being detected in the head/tail of the chain and in the branches of the middle section. We have proved that a coexistence phase with a delocalized domain wall may exist not only in simple chains between reservoirs of low and high density, but also between chains in the maximum current phase.

In the next two works [36, 37] we continued with the study of the above network, however we studied what happens when the double section is moved from the central position along the network. Results of numerical simulations reveal an interesting feature of the network: when the current through the system takes its maximum value, a simple translation of the double-chain section forward or backward along the network leads to a sharp change in the shape of the density profiles in the parallel chains, thus affecting the total number of particles in that part of the network. We refer to this transition as position-induced phase change. We applied again ERA to this system to find the phases of the different segments, induced by the translation of the double section. An explanation of the described phenomenon of phase change on the middle chains $C_{2,3}$ is offered in terms of a finite-size dependence of the effective injection and ejection rates α_d^* and β_d^* at the ends of the double-chain section, thus producing a combined effect on the phase state of the middle branches. We present here also results of numerical simulations for a similar system (however when the total length of the system is not preserved) when a simple change of the length of the head or tail simple chain segment induces similar change in the phase states of the middle branches.

Then, in [38, 39] we extended ERA approach for the study of TASEP with shortcuts of zero length and arbitrary length, and obtained new interesting results concerning stationary non-equilibrium states of the TASEP in these cases. For the considered model of shortcut with zero length and arbitrary length we have found the conditions for existence of a shock phase. Due to the finite-size effects of the effective rates, for all values of the external rates in the domain of Maximal Current phase, there exists a position of the shortcut, where the shunted segment is in a shock phase with completely delocalized domain wall. The shift of the shortcut from this position to the head or tail segment of the network leads to a phase change in the shunted segment to a high-density or to a low-density phase, respectively.

We have shown that in the case of a zero-length shortcut, the effective injection and ejection rates satisfy a cubic equation with coefficients linearly depending on the probability of choosing the shortcut.

In fact, the shortcut in an open network at the maximum current decreases the current in the shunted segment to a value, which can be supported in a low- or high-density phase, or on the coexistence line between these. We showed that the main

features of the coexistence phase depend only on the current through the shortcut.

Unexpected results are that: a) the creation of a shortcut in a directed track may cause a traffic jam in both the shunted section and in the shortcut itself, b) that the completely delocalized domain wall in the shock phase of the shunted segment induces similar behavior in a shortcut with the shortcut with a small number of sites.

The presented results, observed in the different variants of the networks considered in our works, might have interesting implications for the traffic flow control as well as for biological transport processes in living cells. In application to vehicular traffic the results may suggest optimal solutions for planning of road shortcuts. Therefore, the interest in such studies is quite predictable. That is why complex networks have been a focus of intense research in the past thirty years. At the same time, the constantly increasing technical resources make research very encouraging especially when combined with appropriately developed theoretical methods for analyzing more complex systems.

ACKNOWLEDGEMENTS

The results presented here are largely inspired by our dear colleague Prof. J. G. Brankov and obtained in close collaboration with him. The authors gratefully acknowledge also fruitful discussions with their late colleague Prof. V. B. Priezzhev. Partial financial supports by the Bulgarian MES through Grant No. D01-221/03.12. 2018 for NCDSC—part of the Bulgarian National Roadmap on RIs, and by the Plenipotentiary Representative of the Bulgarian Government at JINR, Dubna, through grant No. 01-3-1137-2019/2023 (and also through the BNR on RIs) are thankfully acknowledged.

REFERENCES

[1] NATIONAL RESEARCH COUNCIL (2007) "Condensed-Matter and Materials Physics: The Science of the World Around Us". Washington, DC: The National Academies Press; DOI: https://doi.org/10.17226/11967.

[2] BASIC ENERGY SCIENCES ADVISORY COMMITTEE (2007) "Directing Matter and Energy: Five Challenges for Science and the Imagination". Washington, DC, USA: Department of Energy Publications.

[3] S. KATZ, J.L. LEBOWITZ, H. SPOHN (1983) Phase transitions in stationary nonequilibrium states of model lattice systems. *Physical Review B* **28** 1655; DOI: https://doi.org/10.1103/PhysRevB.28.1655.

[4] S. KATZ, J.L. LEBOWITZ, H. SPOHN (1984) Nonequilibrium steady states of stochastic lattice gas models of fast ionic conductors. *Journal of Statistical Physics* **34** 497-537: DOI: https://doi.org/10.1007/BF01018556.

[5] C.T. MacDonald, J.H. Gibbs, A.C. Pipkin (1968) Kinetics of biopolymerization on nucleic acid templates. *Biopolymers* **6** 1; DOI: https://doi.org/10.1002/bip.1968.360060102.

[6] F. Spitzer (1970) Interaction of Markov processes. *Advances in Mathematics* **5** 246-290.

[7] T. Tripathi, D. Chowdhury (2008) Interacting RNA polymerase motors on a DNA track: Effects of traffic congestion and intrinsic noise on RNA synthesis. *Physical Review E* **77** 011921; DOI: https://doi.org/10.1103/PhysRevE.77.011921.

[8] S. Klump, R. Lipowsky (2003) Traffic of Molecular Motors Through Tube-Like Compartments. *Journal of Statistical Physics* **113** 233; DOI: https://doi.org/10.1023/A:1025778922620.

[9] D. Chowdhury, L. Santen, A. Schadschneider (2000) Statistical physics of vehicular traffic and some related systems. *Physics Reports* **329** 199; DOI: https://doi.org/10.1016/S0370-1573(99)00117-9.

[10] K. Nagle (1996) Particle hopping models and traffic flow theory. *Physical Review E* **53** 4655; DOI: https://doi.org/10.1103/PhysRevE.53.4655.

[11] D. Helbing (2001) Traffic and related self-driven many-particle systems. *Reviews of Modern Physics* **73** 1067; DOI: https://doi.org/10.1103/RevModPhys.73.1067.

[12] P. Greulich, A. Garai, K. Nishinari, A. Schadschneider, D. Chowdhury (2007) Intracellular transport by single-headed kinesin KIF1A: Effects of single-motor mechanochemistry and steric interactions. *Physical Review E* **75** 041905; DOI: https://doi.org/10.1103/PhysRevE.75.041905.

[13] A.B. Kolomeisky (2007) Channel-Facilitated Molecular Transport across Membranes: Attraction, Repulsion, and Asymmetry. *Physical Review Letters* **98** 048105; https://doi.org/10.1103/PhysRevLett.98.048105.

[14] A. Zilman, J. Pearson, G. Bel (2009) Effects of Jamming on Nonequilibrium Transport Times in Nanochannels. *Physical Review Letters* **103** 128103; DOI: https://doi.org/10.1103/PhysRevLett.103.128103.

[15] K. Nagel, M. Schreckenberg (1992) A cellular automaton model for freeway traffic. *Journal de Physique I, EDP Sciences* **2** 2221-2229; DOI: https://doi.org/0.1051/jp1:1992277

[16] B. Derrida, E. Domany, D. Mukamel (1992) An exact solution of a one-dimensional asymmetric exclusion model with open boundaries. *Journal of Statistical Physics* **69** 867; DOI: https://doi.org/10.1007/BF01050430.

[17] G. Schütz, E. Domany (1993) Phase transitions in an exactly soluble one-dimensional exclusion process. *Journal of Statistical Physics* **72** 277; DOI: https://doi.org/10.1007/BF01048050.

[18] B. Derrida, M.R. Evans, V. Hakim, V. Pasquier (1993) Exact solution of a 1D asymmetric exclusion model using a matrix formulation *Journal of Physics A: Mathematical and General* **26** 1493; DOI: https://doi.org/10.1088/0305-4470/26/7/011.

[19] H. HINRICHSEN (1996) Matrix product ground states for exclusion processes with parallel dynamics. *Journal of Physics A: Mathematical and General* **29** 3659; DOI: https://doi.org/10.1088/0305-4470/29/13/030.

[20] N. RAJEWSKY1, A. SCHADSCHNEIDER, M. SCHRECKENBERG (1996) The asymmetric exclusion model with sequential update. *Journal of Physics A: Mathematical and General* **29** L305; DOI: https://doi.org/10.1088/0305-4470/29/12/004.

[21] M.R. EVANS, N. RAJEWSKY, E.R. SPEER (1999) Exact Solution of a Cellular Automaton for Traffic. *Journal of Statistical Physics* **95** 45-96; DOI: https://doi.org/10.1023/A:1004521326456.

[22] J. DE GIER, B. NIENHUIS (1999) Exact stationary state for an asymmetric exclusion process with fully parallel dynamics. *Physical Review E* **59** 4899-4911; DOI: https://doi.org/10.1103/PhysRevE.59.4899.

[23] J. KRUG (1991) Boundary-induced phase transitions in driven diffusive systems. *Physical Review Letters* **67** 1882-1885; DOI: https://doi.org/10.1103/PhysRevLett.67.1882.

[24] G.M. SCHÜTZ (2001) Exactly Solvable Models for Many-Body Systems Far from Equilibrium. In: C. Domb, J.L. Lebowitz (eds.) "Phase Transitions and Critical Phenomena", Vol. 19. Academic Press, London Sydney Tokyo, pp. 1-251.

[25] M.R. EVANS, T. HANNEY (2005) Nonequilibrium statistical mechanics of the zero-range process and related models. *Journal of Physics A: Mathematical and General* **38** 195-240; DOI: https://doi.org/10.1088/0305-4470/38/19/R01.

[26] S. JANOWSKY, J. LEBOWITZ (1992) Finite size effects and shock fluctuations in the asymmetric simple exclusion process. *Physical Review A* **45** 618-625; DOI: https://doi.org/10.1088/0305-4470/38/19/R01.

[27] S. JANOWSKY, J. LEBOWITZ (1994) Exact results for the asymmetric simple exclusion process with a blockage. *Journal of Statistical Physics* **77** 35-51; DOI: https://doi.org/10.1007/BF02186831.

[28] A. JINDAL, T. MIDHA, A.K. GUPTA (2020) Analysis of interactions in totally asymmetric exclusion process with site-dependent hopping rates: Theory and simulations. *Journal of Physics A* **53** 235001; DOI: https://doi.org/10.1088/1751-8121/ab8a03.

[29] BAHADORAN, T. BODINEAU (2015) Properties and conjectures for the flux of TASEP with site disorder. *Brazilian Journal of Probability and Statistics* **29** 282-312; DOI: 10.1214/14-BJPS277.

[30] C. ARITA, M.E. FOULAADVAND, L. SANTEN (2017) Signal optimization in urban transport: A totally asymmetric simple exclusion process with traffic lights. *Physical Review E* **95** 032108; DOI: https://doi.org/10.1103/PhysRevE.95.032108.

[31] A. JINDAL, A.B. KOLOMEISKY, A.K. GUPTA (2020) The role of dynamic defects in transport of interacting molecular motors. *Journal of Statistical Mechanics: Theory and Experiment* **2020** 043206; DOI: https://doi.org/10.1088/1742-5468/ab7756.

[32] J. BRANKOV, N. PESHEVA, N. BUNZAROVA (2004) Totally asymmetric exclusion process on chains with a double-chain section in the middle: Computer simulations and a simple theory. *Physical Review E* **69** 066128; DOI: https://doi.org/10.1103/PhysRevE.69.066128.

[33] J. BRANKOV, N. PESHEVA, N. BUNZAROVA (2005) One-Dimensional Traffic Flow Models: Theory and Computer Simulations. In: *Proceedings of the 10th Jubilee National Congress on Theoretical and Applied Mechanics*, Varna, 13-16 September 2005, Vol. 1, pp. 442-456. (Available also at arXiv:0803.2625 [cond-mat.stat-mech])

[34] I. NERI, N. KERN, A. PARMEGGIANI (2011) TASEP transport on networks: Theory for strongly connected networks. *Physical Review Letters* **107** 068702; DOI: https://doi.org/10.1103/PhysRevLett.107.068702.

[35] Y. BAEK, M. HA, H. JEONG (2014) Effects of junctional correlations in the totally asymmetric simple exclusion process on random regular networks. *Physical Review E* **90** 062111; DOI: https://doi.org/10.1103/PhysRevE.90.062111.

[36] N. PESHEVA, J. BRANKOV (2012) Position-induced phase change in a TASEP with a double-chain section (a model of biological transport). *Biomath Forum* **1** 2; DOI: http://dx.doi.org/10.11145/j.biomath.2012.11.211.

[37] N. PESHEVA, J. BRANKOV (2013) Position dependence of the particle density in a double-chain section of a linear network in a totally asymmetric simple exclusion process. *Physical Review E* **87** 062116; DOI: https://doi.org/10.1103/PhysRevE.87.062116.

[38] N. BUNZAROVA, N. PESHEVA, J. BRANKOV (2014) Asymmetric simple exclusion process on chains with a shortcut. *Physical Review E* **89** 032125; DOI: https://doi.org/10.1103/PhysRevE.89.032125.

[39] N. BUNZAROVA, N. PESHEVA, J. BRANKOV (2015) On the appearance of traffic jams in a long chain with a shortcut in the bulk. *Physica A: Statistical Mechanics and its Applications* **438** 645-656; DOI: https://doi.org/10.1016/j.physa.2015.07.013.

[40] M. WÖLKI (2005) Steady States of Discrete Mass Transport Models. Master thesis, University of Duisburg-Essen.

[41] A.E. DERBYSHEV, S.S. POGHOSYAN, A.M. POVOLOTSKY, V.B. PRIEZZHEV (2012) The totally asymmetric exclusion process with generalized update. *Journal of Statistical Mechanics: Theory and Experiment* **2012** 05014; DOI: https://doi.org/10.1088/1742-5468/2012/05/P05014.

[42] P. HRABÁK (2014) Ph.D. Thesis. Czech Technical University in Prague. Faculty of Nuclear Sciences and Physical Engineering. Praga.

[43] A.E. DERBYSHEV, A.M. POVOLOTSKY, V.B. PRIEZZHEV (2015) Emergence of jams in the generalized totally asymmetric simple exclusion process. *Physical Review E* **91** 022125; DOI: https://doi.org/10.1103/PhysRevE.91.022125.

[44] B.L. ANEVA, J.G. BRANKOV (2016) Matrix-product ansatz for the totally asymmetric simple exclusion process with a generalized update on a ring. *Physical Review E* **94** 022138; DOI: https://doi.org/10.1103/PhysRevE.94.022138.

[45] N.ZH. BUNZAROVA, N.C. PESHEVA (2017) One-dimensional irreversible aggregation with dynamics of a totally asymmetric simple exclusion process. *Physical Review E* **95** 052105; DOI: https://doi.org/10.1103/PhysRevE.95.052105.

[46] J.G. BRANKOV, N.ZH. BUNZAROVA, N.C. PESHEVA, V.B. PRIEZZHEV (2018) A model of irreversible jam formation in dense traffic. *Physica A: Statistical Mechanics and its Applications* **494** 340; DOI: https://doi.org/10.1016/j.physa.2017.11.158.

[47] N.ZH. BUNZAROVA, N.C. PESHEVA, V.B. PRIEZZHEV, J.G. BRANKOV (2017) A model of jam formation in congested trafic. *Journal of Physics: Conference Series* **936** 012026; DOI: https://doi.org/10.1088/1742-6596/936/1/012026.

[48] N.ZH. BUNZAROVA, N.C. PESHEVA, J.G. BRANKOV (2019) One-dimensional discrete aggregation-fragmentation model. *Physical Review E* **100** 0022145; DOI: https://doi.org/10.1103/PhysRevE.100.022145.

[49] B. PAL, A.K. GUPTA (2002) Role of interactions in a closed quenched system. *Journal of Physics A: Mathematical and Theoretical* **54** 2; DOI: https://doi.org/10.1088/1751-8121/abcf0e.

[50] L. GRÜNE, T. KRIECHERBAUER, M. MARGALIOT (2020) Random attraction in the TASEP model. *SIAM Journal on Applied Dynamical Systems* **20**(1) 65-93; DOI: https://doi.org/10.1137/20M131446X.

[51] L.J. COOK, R.K.P. ZIA (2009) Feedback and fluctuations in a totally asymmetric simple exclusion process with finite resources. *Journal of Statistical Mechanics: Theory and Experiment* **2009** P02012; DOI: https://doi.org/10.1088/1742-5468/2009/02/P02012.

[52] P. GREULICH, L. CIANDRINI, R.J. ALLEN, M.C. ROMANO (2012) Mixed population of competing totally asymmetric simple exclusion processes with a shared reservoir of particles. *Physical Review E* **85** 011142; DOI: https://doi.org/10.1103/PhysRevE.85.011142.

[53] C.A. BRACKLEY, L. CIANDRINI, M.C. ROMANO (2012) Multiple phase transitions in a system of exclusion processes with limited reservoirs of particles and fuel carriers. *Journal of Statistical Mechanics: Theory and Experiment* **2012** P03002; DOI: https://doi.org/10.1088/1742-5468/2012/03/P03002.

[54] E. PRONINA, A.B. KOLOMEISKY (2005) Theoretical investigation of totally asymmetric exclusion processes on lattices with junctions. *Journal of Statistical Mechanics: Theory and Experiment* **2005** P07010; DOI: https://doi.org/10.1088/1742-5468/2005/07/P07010.

[55] A.B. KOLOMEISKY, G.M. SCHÜTZ, E.B. KOLOMEISKY J.P. STRALEY (1998) Phase diagram of one-dimensional driven lattice gases with open boundaries. *Journal of Physics A: Mathematical and General* **31** 6911; DOI: https://doi.org/10.1088/0305-4470/31/33/003.

[56] L. SANTEN, C. APPERT (2002) The Asymmetric Exclusion Process Revisited: Fluctuations and Dynamics in the Domain Wall Picture. *Journal of Statistical Physics* **106** 187; DOI: https://doi.org/10.1023/A:1013176229983.

[57] N. RAJEWSKI, M. SCHRECKENBERG (1997) Exact results for one-dimensional cellular automata with different types of updates. *Physica A: Statistical Mechanics and its Applications* **245** 139-144; DOI: https://doi.org/10.1016/S0378-4371(97)00010-1.

[58] N. RAJEWSKI, L. SANTEN, A. SCHADSCHNEIDER, M. SCHRECKENBERG (1998) The asymmetric exclusion process: Comparison of update procedures. *Journal of Statistical Physics* **92** 151-194; DOI: https://doi.org/10.1023/A:1023047703307.

[59] B. EMBLEY, A. PARMEGGIANI, N. KERN (2009) Understanding totally asymmetric simple-exclusion-process transport on networks: Generic analysis via effective rates and explicit vertices. *Physical Review E* **80** 041128; DOI: https://doi.org/10.1103/PhysRevE.80.041128.

[60] Z.P. CAI, Y.M. YUAN, R. JIANG, M.B. HU (2008) Asymmetric coupling in multichannel simple exclusion processes. *Journal of Statistical Mechanics Theory and Experiment* **2008** P07016; DOI: https://doi.org/10.1088/1742-5468/2008/07/P07016.

[61] X. WANG, R. JIANG, M.B. HU, K. NISHINARI (2009) Totally Asymmetric Exclusion Processes on Lattices with a Branching Point. *International Journal of Modern Physics C* **20** 1999-2012; DOI: https://doi.org/10.1142/S0129183109014886.

[62] T. TANNAI, K. NISHINARI (2017) Theoretical approach to congestion relaxation and saturated congestion in TASEP (totally asymmetric simple exclusion process) network with multi-chain section with flow/density-dependent rules of junctions. *Physics Letters A* **38** 3688-3695; DOI: https://doi.org/10.1016/j.physleta.2017.09.034.

[63] Y.-M. YUAN, R. JIANG, R. WANG, M.-B. HU, Q.-S. WU (2017) Totally asymmetric simple exclusion process with a shortcut. *Journal of Physics A: Mathematical and Theoretical* **40** 12351; DOI: https://doi.org/10.1088/1751-8113/40/41/006.